(12)

DNA-TR-86-214

INTERACTIONS AND SPREADING OF ADJACENT LARGE AREA FIRES

D. Weihs
R.D. Small
Pacific-Sierra Research Corporation
12340 Santa Monica Blvd
Los Angeles, CA 90025-2587

31 March 1986

Technical Report

CONTRACT No. DNA 001-85-C-0089

THIS WORK WAS SPONSORED BY THE DEFENSE NUCLEAR AGENCY
UNDER RDT&E RMC CODE B3110854662 RD RB 00119 25904D.

Prepared for
Director
DEFENSE NUCLEAR AGENCY
Washington, DC 20305-1000

Destroy this report when it is no longer needed. Do not return to sender.

PLEASE NOTIFY THE DEFENSE NUCLEAR AGENCY, ATTN: STTI, WASHINGTON, DC 20305-1000, IF YOUR ADDRESS IS INCORRECT, IF YOU WISH IT DELETED FROM THE DISTRIBUTION LIST, OR IF THE ADDRESSEE IS NO LONGER EMPLOYED BY YOUR ORGANIZATION.

DISTRIBUTION LIST UPDATE

This mailer is provided to enable DNA to maintain current distribution lists for reports. We would appreciate your providing the requested information.

☐ Add the individual listed to your distribution list.

☐ Delete the cited organization/individual.

☐ Change of address.

NAME: _____

ORGANIZATION: _____

OLD ADDRESS	CURRENT ADDRESS
_____	_____
_____	_____
_____	_____

TELEPHONE NUMBER: ( ) _____

SUBJECT AREA(s) OF INTEREST:

_____	_____
_____	_____
_____	_____

DNA OR OTHER GOVERNMENT CONTRACT NUMBER: _____

CERTIFICATION OF NEED-TO-KNOW BY GOVERNMENT SPONSOR (if other than DNA):

SPONSORING ORGANIZATION: _____

CONTRACTING OFFICER OR REPRESENTATIVE: _____

SIGNATURE: _____

Director
Defense Nuclear Agency
ATTN: STTI
Washington, DC 20305-1000

Director
Defense Nuclear Agency
ATTN: STTI
Washington, DC 20305-1000

UNCLASSIFIED
SECURITY CLASSIFICATION OF THIS PAGE

AD-A176 338

REPORT DOCUMENTATION PAGE

1a. REPORT SECURITY CLASSIFICATION UNCLASSIFIED	1b. RESTRICTIVE MARKINGS
2a. SECURITY CLASSIFICATION AUTHORITY N/A since Unclassified	3 DISTRIBUTION/AVAILABILITY OF REPORT Approved for public release; distribution is unlimited.
2b. DECLASSIFICATION/DOWNGRADING SCHEDULE N/A since Unclassified	
4 PERFORMING ORGANIZATION REPORT NUMBER(S) PSR Note 719	5. MONITORING ORGANIZATION REPORT NUMBER(S) DNA-TR-86-214
6a. NAME OF PERFORMING ORGANIZATION Pacific-Sierra Research Corporation 6b. OFFICE SYMBOL (If applicable)	7a. NAME OF MONITORING ORGANIZATION Director Defense Nuclear Agency
6c. ADDRESS (City, State, and ZIP Code) 12340 Santa Monica Boulevard Los Angeles, California 90025-2587	7b. ADDRESS (City, State, and ZIP Code) Washington, DC 20305-1000
8a. NAME OF FUNDING/SPONSORING ORGANIZATION 8b. OFFICE SYMBOL (If applicable) SPTD	9 PROCUREMENT INSTRUMENT IDENTIFICATION NUMBER DNA 001-85-C-0089
8c. ADDRESS (City, State, and ZIP Code)	10. SOURCE OF FUNDING NUMBERS PROGRAM ELEMENT NO. 62715H; PROJECT NO RD; TASK NO. RB; WORK UNIT ACCESSION NO. DH00119

11. TITLE (Include Security Classification)
INTERACTIONS AND SPREADING OF ADJACENT LARGE AREA FIRES

12. PERSONAL AUTHOR(S)
Weihs, D.; Small, R. D.

13a. TYPE OF REPORT	13b. TIME COVERED	14. DATE OF REPORT (Year, Month, Day)	15. PAGE COUNT
Technical	FROM 841115 TO 860331	860331	46

16. SUPPLEMENTARY NOTATION
This work was sponsored by the Defense Nuclear Agency under RDT&E RMC Code B3110854662 RD RB 00119 25904D.

17 COSATI CODES			18. SUBJECT TERMS (Continue on reverse if necessary and identify by block number)
FIELD	GROUP	SUB-GROUP	Fire Fronts, Multiburst
18	3		Fire Spread, Multiple Fires,
13	12		Large Area Fires, Urban Fires

19. ABSTRACT (Continue on reverse if necessary and identify by block number)

Multiple nuclear weapon bursts in an urban area could lead to separate large area fires. If sufficiently far apart, each fire burns independently and little, if any, fire spread is expected. For small separations, the flow fields generated by each fire can interact and fire spread may result. Singularity theory is used to model the flow field generated by a single large area fire. The defined singularity distribution is based on theoretical and numerical solutions for large area fires. Several distributions are used to simulate the effect of multiple nuclear weapon bursts in an urban area. For some placements, the area fires remain independent. Spread and merging of area fires is indicated in several examples. The results suggest that multiple bursts can lead to merging of area fires and thus greatly increased burnout areas.

20. DISTRIBUTION/AVAILABILITY OF ABSTRACT ☐ UNCLASSIFIED/UNLIMITED ☒ SAME AS RPT ☐ OTIC USERS	21 ABSTRACT SECURITY CLASSIFICATION UNCLASSIFIED
22a. NAME OF RESPONSIBLE INDIVIDUAL Betty L. Fox	22b. TELEPHONE (Include Area Code) (202)325-7042 22c. OFFICE SYMBOL DNA/STTI

DD FORM 1473, 84 MAR 83 APR edition may be used until exhausted. All other editions are obsolete.

SECURITY CLASSIFICATION OF THIS PAGE
UNCLASSIFIED

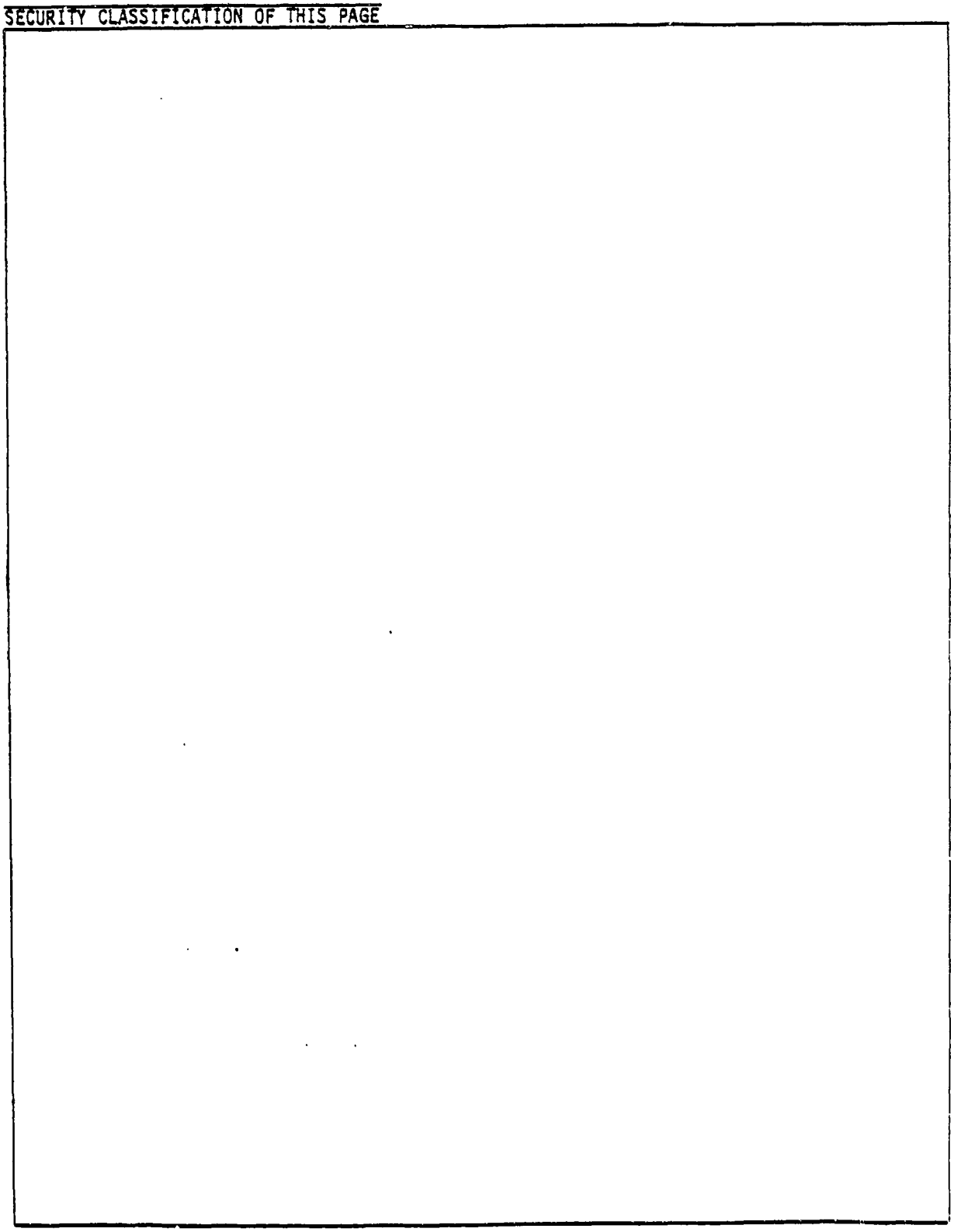

PREFACE

This report was prepared by Pacific-Sierra Research Corporation (PSR), a wholly owned subsidiary of Eaton Corporation, for the Defense Nuclear Agency (DNA). The work was done under contract DNA 001-85-C-0089, and supervised by Dr. Michael J. Frankel.

In previous PSR studies, the physics of a single large area fire has been considered. In this note, the interaction between two or more large area fires is analyzed. Sample results illustrate the spreading and merging that can occur in a multiple burst environment.

CONVERSION TABLE

Conversion factors for U.S. Customary to metric (SI) units of measurement

MULTIPLY → BY → TO GET TO GET ← BY ← DIVIDE		
angstrom	1.000 000 X E -10	meters (m)
atmosphere (normal)	1.013 25 X E +2	kilo pascal (kPa)
bar	1.000 000 X E +2	kilo pascal (kPa)
barn	1.000 000 X E -28	meter^2 (m^2)
British thermal unit (thermochemical)	1.054 350 X E +3	joule (J)
calorie (thermochemical)	4.184 000	joule (J)
cal (thermochemical)/cm^2	4.184 000 X E -2	mega joule/m^2 (MJ/m^2)
curie	3.700 000 X E +1	*giga becquerel (GBq)
degree (angle)	1.745 329 X E -2	radian (rad)
degree Fahrenheit	$t_k = (t°f + 459.67)/1.8$	degree kelvin (K)
electron volt	1.602 19 X E -19	joule (J)
erg	1.000 000 X E -7	joule (J)
erg/second	1.000 000 X E -7	watt (W)
foot	3.048 000 X E -1	meter (m)
foot-pound-force	1.355 818	joule (J)
gallon (U.S. liquid)	3.785 412 X E -3	meter^3 (m^3)
inch	2.540 000 X E -2	meter (m)
jerk	1.000 000 X E +9	joule (J)
joule/kilogram (J/kg) (radiation dose absorbed)	1.000 000	Gray (Gy)
kilotons	4.183	terajoules
kip (1000 lbf)	4.448 222 X E +3	newton (N)
kip/inch^2 (ksi)	6.894 757 X E +3	kilo pascal (kPa)
ktap	1.000 000 X E +2	newton-second/m^2 ($N-s/m^2$)
micron	1 000 000 X E -6	meter (m)
mil	2.540 000 X E -5	meter (m)
mile (international)	1.609 344 X E +3	meter (m)
ounce	2.834 952 X E -2	kilogram (kg)
pound-force (lbs avoirdupois)	4.448 222	newton (N)
pound-force inch	1.129 848 X E -1	newton-meter (N·m)
pound-force/inch	1.751 268 X E +2	newton/meter (N/m)
pound-force/foot^2	4.788 026 X E -2	kilo pascal (kPa)
pound-force/inch^2 (psi)	6.894 757	kilo pascal (kPa)
pound-mass (lbm avoirdupois)	4.535 924 X E -1	kilogram (kg)
pound-mass-foot^2 (moment of inertia)	4.214 011 X E -2	kilogram-meter^2 ($kg·m^2$)
pound-mass/foot^3	1.601 846 X E +1	kilogram/meter^3 (kg/m^3)
rad (radiation dose absorbed)	1.000 000 X E -2	**Gray (Gy)
roentgen	2.579 760 X E -4	coulomb/kilogram (C/kg)
shake	1.000 000 X E -8	second (s)
slug	1.459 390 X E +1	kilogram (kg)
torr (mm Hg, 0° C)	1.333 22 X E -1	kilo pascal (kPa)

*The becquerel (Bq) is the SI unit of radioactivity; 1 Bq = 1 event/s.
**The Gray (Gy) is the SI unit of absorbed radiation.

TABLE OF CONTENTS

LIST OF ILLUSTRATIONS

SECTION 1
INTRODUCTION

A single area fire started by a nuclear weapon burst is likely to have a well-defined boundary and little, if any, increase in the fire area In the few recorded area fires, spread did not occur [Bond, 1946; Irving, 1963; and Miller, 1968]; the high-velocity fire winds generated by the strong buoyancy of the area fires [Small and Larson, 1986] limited the outward spread. Unless the ambient wind velocity is greater than the induced fire-wind velocity, the area fire system is likely to be stable and not grow. There can, of course, be exceptions due to topography, uneven fuel loadings, or local instabilities at the fire boundary (fingering) that could lead to changes in the perimeter. In general, stable fronts are expected for single area fires.

The fire-wind velocity is greatest at the fire perimeter and decreases slowly with distance from the fire. This is for a mature fire--one that has burned long enough to establish a far field. (Such fires are more likely to occur in urban areas than in wildlands due to the larger fuel concentrations in an urban area and correspondingly longer burning times.) Calculations show that velocities on the order of 1 m/s are possible at 3 to 4 fire radii. Such far-field velocities are large enough that separate area fires could interact if spaced sufficiently close to each other.

In many urban areas, potential targets are widely spaced (in terms of weapon radii) and multiple bursts are likely. Thus, several area fires could develop. Initially, each area fire would burn independently; however, as the flow fields develop, interactions leading to changes in the fire boundary are possible. The area fires could merge; smaller or weaker fires migrating toward the larger or more intense fires.

In this report, we consider the interactions of multiple large area fires separated by distances on the order of a fire diameter, and

determine when fire spread is probable for some simple lay downs. A simple, analytical model of the fire plume and its effects on the surroundings is developed. Distributions of singularities such as sinks, sources, and vortices are then defined such that the flow field induced by a single large area fire [Small, Remetch, and Brode, 1984] is reproduced. Although basically inviscid, the model effectively accounts for viscous effects.

Next, two or more such distributions are placed in close proximity and the interactive influence on the fire winds and the spreading smoke plume flow fields are calculated. This simplified model is used to approximate the interaction effects without recourse to hydrocode solution of the three-dimensional unsteady Navier-Stokes equations. We specifically study the ways in which nearby fires and their associated flow fields can promote the spreading of an initially circular, uniformly burning area. The present results reproduce, at least qualitatively, the direction of changes in individual fire boundaries due to neighboring fires.

SECTION 2
ANALYSIS OF AN ISOLATED AREA FIRE

Large area fires, defined such that the radius of the burning area is on the order of the atmospheric thickness [$O(10^4$ m)], produce a typical flow field consisting of a ground level inflow of air, a flame zone of radius R and height H_f, a buoyant plume of combustion gases and smoke moving upwards (with possible crosswind effects), air entrained from around the plume, and a spreading "fountain" at the plume equilibrium height H at which the plume gases are in equilibrium. That pattern is obtained by relatively high resolution calculations of the time-dependent, viscous, buoyant flow field [Small, Remetch, and Brode, 1984]. Similar hydrocode solutions have shown relatively good agreement with observations and data from scale experiments [Small, 1985] and the Flambeau tests [Nielsen, 1970].

The flow field of an isolated fire outside of the burning zone ($r > R$) is modeled by a vertical distribution of horizontal planar sources and sinks placed at the fire centerline, with sinks at the lower parts to generate inflow and sources at the top (see Fig. 1). That approach is consistent with the observation of Smith, Morton, and Leslie [1975] and Cox and Chitty [1980] of a "sink-like" inflow at ground level, for large fires. Swirl could be easily included by adding a vortex with vertical axis. That would not affect the sink model at ground level--the flow remains essentially radial even if strong swirl exists [Emmons, 1965]. Moreover, we have recently shown that a large plume is not likely to swirl [Weihs and Small, 1985].

The singularity strength is modeled by a combination of "basic" sinks that describe the fire requirements and "entrainment" sinks that model the added entrained (plume) flow.

The strength of the basic sinks is obtained from the energy per unit time Q_F produced by a fire of radius R. This is

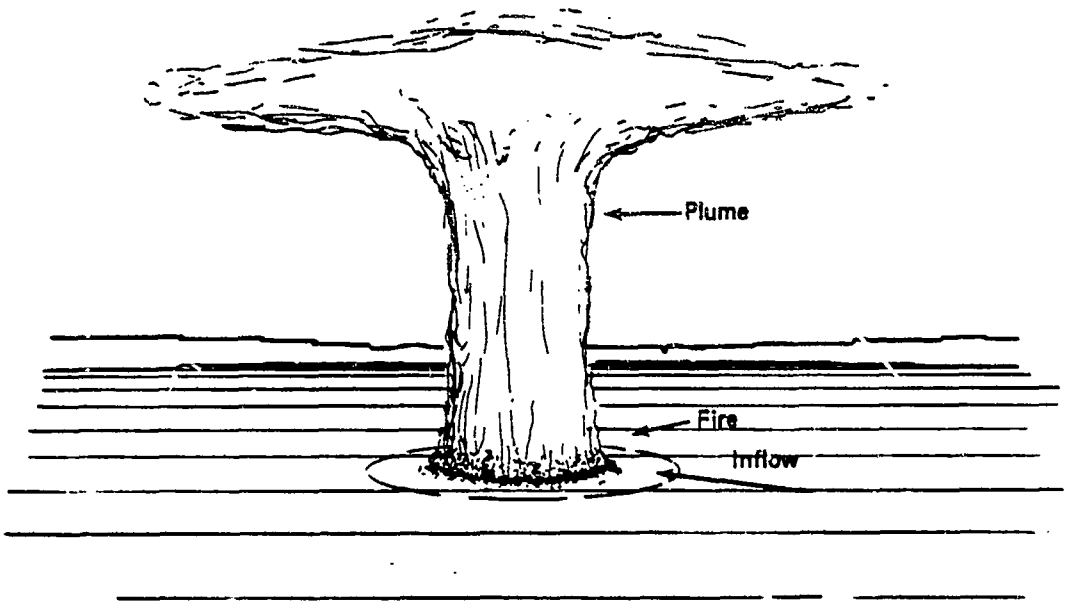

a. Axonometric description of fire and plume.

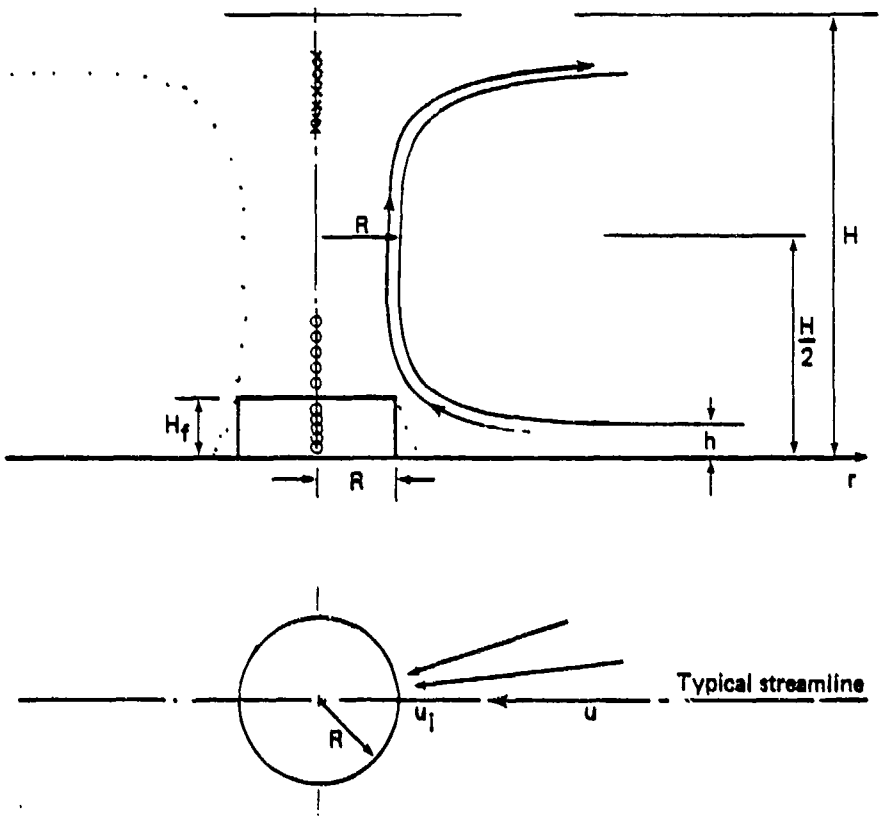

b. Vertical section through fire center and description of coordinates, parameters, and model singularities.

Note: Burning zone height is greatly exaggerated to show detail.

Figure 1. Schematic representation of large area fire.

$$Q_F = JV_f = \pi R^2 H_f J, \tag{1}$$

where J is the heat addition rate per unit volume. If C is the average caloric value of the combustibles per unit mass, the mass flux of air required to sustain the fire is

$$\dot{A} = S \frac{Q_f}{C} \quad , \tag{2}$$

where S is the air/fuel ratio.

Computations [Small, Remetch, and Brode, 1984] show that the inflow velocity in the area surrounding the fire (the outer flow) is roughly described by an r^{-1} dependence, with no noticeable changes over the first 100 m of altitude. Thus, we assume the basic sinks to be a linear vertical distribution (of an as yet unknown height) of planar sinks. That implies each horizontal section is independent in terms of the horizontal component of flow, i.e., a source or sink at a given height only drives the flow at that height [Lamb, 1945]. The height h is obtained from the computed ground velocities u_g by

$$h = \frac{\dot{A}}{2\pi r u_g \rho_a} = \frac{SQ_f}{2\pi r u_g c \rho_a} \quad , \tag{3}$$

where r is the distance ($r \geq R$) at which u_g is measured. The basic singularity is of strength $B = A/h$ (in square meters per second) distributed over a vertical distance h.

The induced singularities are obtained by calculating the inflow or outflow at greater heights. To estimate the entrained flow we first need to model the fire plume. The large fires described here are unusual in the sense that the ratio of plume height to fire diameter is O(1) or less. Equilibrium of the plume is controlled by crosswinds or gradients in the atmosphere, rather than by entrainment of ambient air. Accordingly, the point source model [Turner, 1973] of

such plumes is inapplicable. Therefore, we rely on the numerical results which indicate that the plume necks down, causing additional inflow which will be modeled as entrainment sinks. The factor ζ describes the necking of the plume, and ζR the local radius. The speed of the basic plume (the moving cylinder) is obtained by equating mass fluxes. Uniform ("top hat") distributions of velocity and temperature across the plume can be used [Nielsen and Tao, 1965] so that

$$U_p = \frac{\dot{A}(S + 1)}{\pi S R^2 \zeta^2} \quad . \tag{4}$$

The normalized plume mass (S + 1) includes the entrained air (fire winds) and the mass of combustion gases. The entrained flow and induced flow around the plume can be modeled either by the distribution of sinks and sources mentioned above or by one or more coplanar vortex rings that induce ground-level inflow and plume-top outflow. The actual physical process is a result of entrainment and fire-generated pressure gradients at the lower levels, and of a plume fountain effect at the top, but both singularity types can describe those outer flows with any level of accuracy by using finer and finer distributions. We use a combination of both, to retrieve the ground-level distribution of inflow (see Fig. 2) and the velocity distribution at the plume circumference.

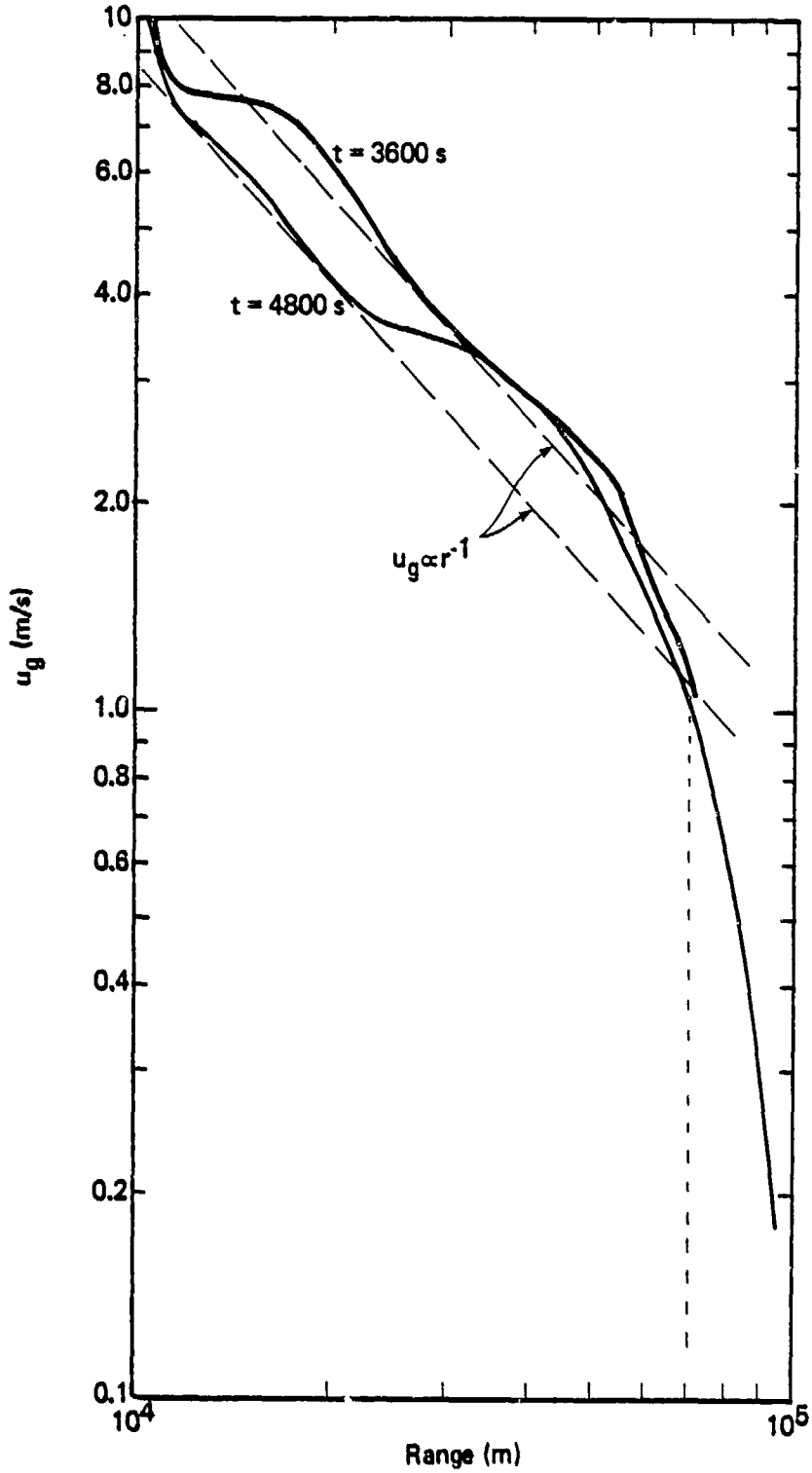

Note: Dashed lines indicate the velocity profile for sinks concentrated at the centerline. Vortex contribution is centered at 1.8×10^4 m at 3600 s and at 3.6×10^4 m at 4800 s.

Source: Small et al. [1984]

Figure 2. Radial inflow velocity at ground level calculated for $R = 10^4$-m fire.

SECTION 3
INTERACTIONS BETWEEN AREA FIRES

To examine the possible spreading of area fires, we consider the effect of a neighboring area fire on the flow field at the perimeter. Large area fires such as those at Hamburg, Dresden, or Hiroshima have exhibited sharply defined bounds of the burnt area, indicating that strong inflow fire winds limit outward spread. This implies that for some minimum radial local inflow velocity, the fire cannot spread. That minimum velocity V_o is a function of the energy density of the fire J, and possibly other parameters such as local curvature of the flame front 1/R, continuity of fuel, etc. The minimum velocity V_o is a necessary, but not sufficient limit (in mathematical terms), i.e., if $0 < |u| < |V_o|$ the fire can, but does not necessarily, spread. For positive ($u > 0$) velocities at the perimeter, we assume the fire will spread.

As a result of the above arguments, it seems that the dominant factors regulating fire spread appear at ground level, within a layer of thickness similar to that of the fire region. As shown previously, the flow in the bottom layer is essentially that of a two-dimensional sink. That will now be applied to the interaction problem. Looking first at fires that are established simultaneously, we consider two, nonequal size fires of sink strengths B_1 and B_2, respectively, where $B_1 \geq B_2$.

For simplicity, we define the length unit as the larger fire radius (i.e., $R_1 = 1$). Then $R_2 = b \leq 1$; the equality sign stands for equal-sized circular fires. The velocities induced by each of the fires independently follow the form

$$u_i = \frac{B_i}{2\pi r_i} ; \quad (r_i \geq R_i) \quad , \tag{5}$$

where r_i represents the radial distance from the respective fire

center. Thus, the speed at a point P on the perimeter of the smaller fire on the line connecting the centers (see Fig. 3) is

$$u_p = \frac{B_1}{2\pi(D - b)} - \frac{B_2}{2\pi b} \quad , \tag{6}$$

where D is the distance between fire centers, normalized by R. When $u_p \geq 0$ the smaller fire tends to spread toward the larger fire. That process is self-amplifying. The outward velocity of the moving area fire is larger because it is closer to the "dominant" fire. For the limiting case ($u_p = 0$),

$$\frac{B_1}{B_2} = \frac{D - b}{b} = \frac{D}{b} - 1 \quad , \tag{7}$$

$$D_m = \left[b\ 1 + \frac{B_1}{B_2} \right], \tag{8}$$

where

$$\left(\frac{B_1}{B_2} \geq 1;\ D_m \geq 1 \right) . \tag{9}$$

When the fires are initially of equal strength ($B_1 = B_2$) $D_m = 2$, the fires merge only if initially touching. For all other cases, there is a finite distance over which the fires tend to combine. The result depends on the fire-induced winds only. Ambient winds may, of course, affect the possibility of outward spread.

A rough estimate can be determined of the distance D_m, as a function of the ratio of fire sizes. we assume both fires to burn similar terrain or urban area, so that the energy addition J and flame height H_f are equal for both. Then, the sink strength B from Eqs. (1) and (3) is proportional to the radius squared, i.e.,

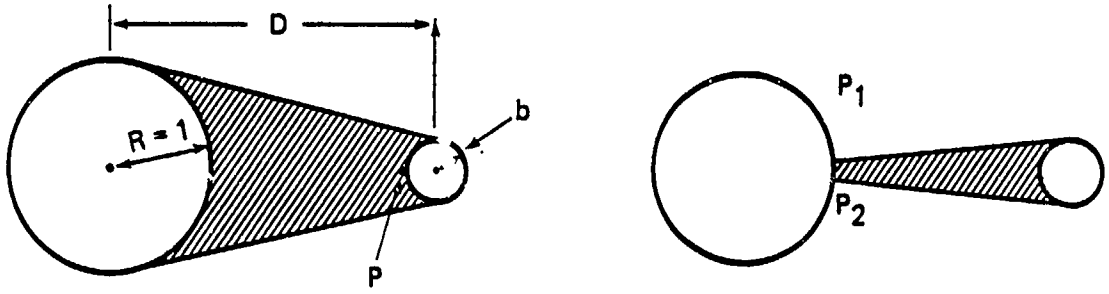

a. Area fires of similar size and strength.

b. Area fires with large difference in size and strength.

Note: Shaded areas indicate spreading zone.

Figure 3. Possible spread patterns for simultaneously burning fires.

$$\frac{B_1}{B_2} = \frac{1}{b^2} \quad , \tag{10}$$

or from Eq. (9),

$$D_m = b + \frac{1}{b} \quad . \tag{11}$$

The limit $b \longrightarrow 0$ implies that a point fire would spread an infinite distance since the large fire serves as an external wind driving the small fire. For the quasi-steady model to be relevant, the speed induced at point P (Fig. 3) should at least be larger than the local turbulent fluctuations (ambient wind or fire generated). Such velocity fluctuations are a higher fraction of the inflow speed, the smaller the fire. Thus, we assume that b should be greater than 0.1.

The changes in area burned due to multiple fire interactions can be obtained by comparing areas for the two fires separately ($\pi + \pi b^2$) and the area included between them (see Fig. 3a). The ratio is

$$F_1 = \frac{\frac{\pi(1 + b^2)}{2} + D(1 + b)}{\pi(1 + b^2)} = \frac{1}{2} + \frac{D}{\pi} \frac{1 + b}{1 + b^2} \quad , \tag{12}$$

and, using Eq. (11)

$$F_1 = \frac{1}{2} + \frac{b + 1}{\pi b} \quad . \tag{13}$$

That can be seen as an upper bound for the interaction, accurate when $b \rightarrow 1$.

When the ratio of initial fire radii is small, a different flow pattern can develop. The inflow toward the larger fire is radial with respect to its center and when the secondary fire is much smaller, a narrowing spread area develops (Fig. 3b). That area is approximately $bD - \pi (\tan^{-1} b/D)$ (when $b < 0.5$) so that the ratio of the merging

system to the initial area fires is

$$F_2 \approx \frac{\frac{\pi b^2}{2} bD + \pi\left(1 - \tan^{-1}\frac{b}{D}\right)}{\pi(1 + b^2)} \quad . \tag{14}$$

The approximatibn results from neglecting parts of the smaller fire circle. The approximation is best for small b, and in Fig. 4, F_2 describes the limit for $b \ll 1$. Substituting Eq. (11) into Eq. (14) we obtain

$$F_2 = \frac{\left(\frac{\pi}{2} + 1\right)b^2 + 1 + \pi\left(1 - \tan^{-1}\frac{b^2}{b^2 + 1}\right)}{\pi(1 + b^2)} \quad , \tag{15}$$

where F_2 tends to a finite limit (≈ 1.32) for $b = 0$ (see Fig. 4). The actual area ratio will probably fall between the curves F_1 (for $b = 1$)

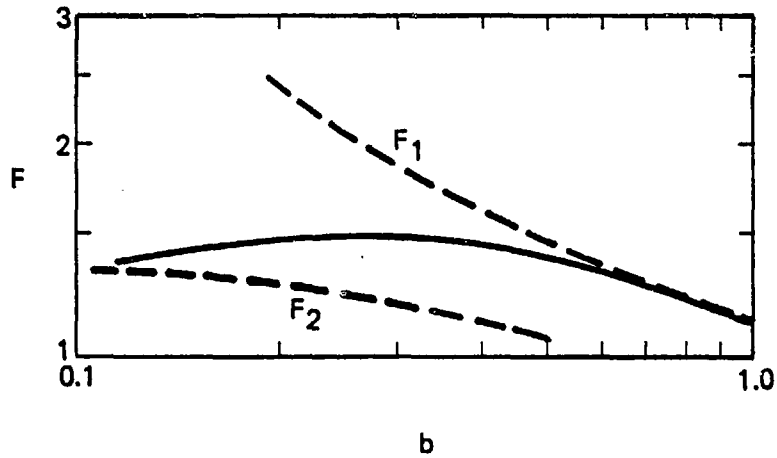

Note: Curve F_1 describes pattern of Fig. 3a, and curve F_2 shows pattern of Fig. 3b. The solid line interpolates between limiting cases.

Figure 4. Ratio of total system fire area to sum of initial area fires F, as function of ratio of individual fire radii.

and F_2 for $(b \longrightarrow 0)$. Thus, an increase of up to 50 percent in area burned due to the interaction is possible for fires with a size ratio of approximately 3, separated by ≈ 3.5 large fire radii (shown schematically in Fig. 3a-b).

The results shown in Fig. 4 consider the merging of area fires when a net nonzero velocity is established between them. This is spread in the wind direction by the weaker fire; one area fire is stationary. Fires can also spread against the wind when the fire-induced speed is less than some minimum V_o. That velocity is a function of the fire shape and strength. The strength influences the updraft and entrainment at the perimeter, which in turn can sweep up fire brands and drop them beyond the fire area. The mechanisms determining a minimum value for V_o are not well established. We thus vary V_o parametrically and examine the area fire interactions. The inflow velocity u_2 at the perimeter of an isolated fire of radius $R_2 = bR_1$ is assumed related to V_o by Ku_2. Therefore, from Eq. (5)

$$V_o = K \frac{B_2}{2\pi b} \quad . \tag{16}$$

From Eq. (6), with $V_o = u_p$, we obtain, after some manipulation,

$$D_m = \frac{1 + (K + 1)b^2}{(K + 1)b} \quad , \tag{17}$$

which reduces to Eq. (11) when $K = 0$, as expected. Essentially, a finite value of V_o does not result in any qualitative changes The range over which interactions are possible is increased and similarly, the spread area is increased (see Fig. 5).

Since area fires have a life span limited by the amount of combustibles available, there is a different limitation on the increase

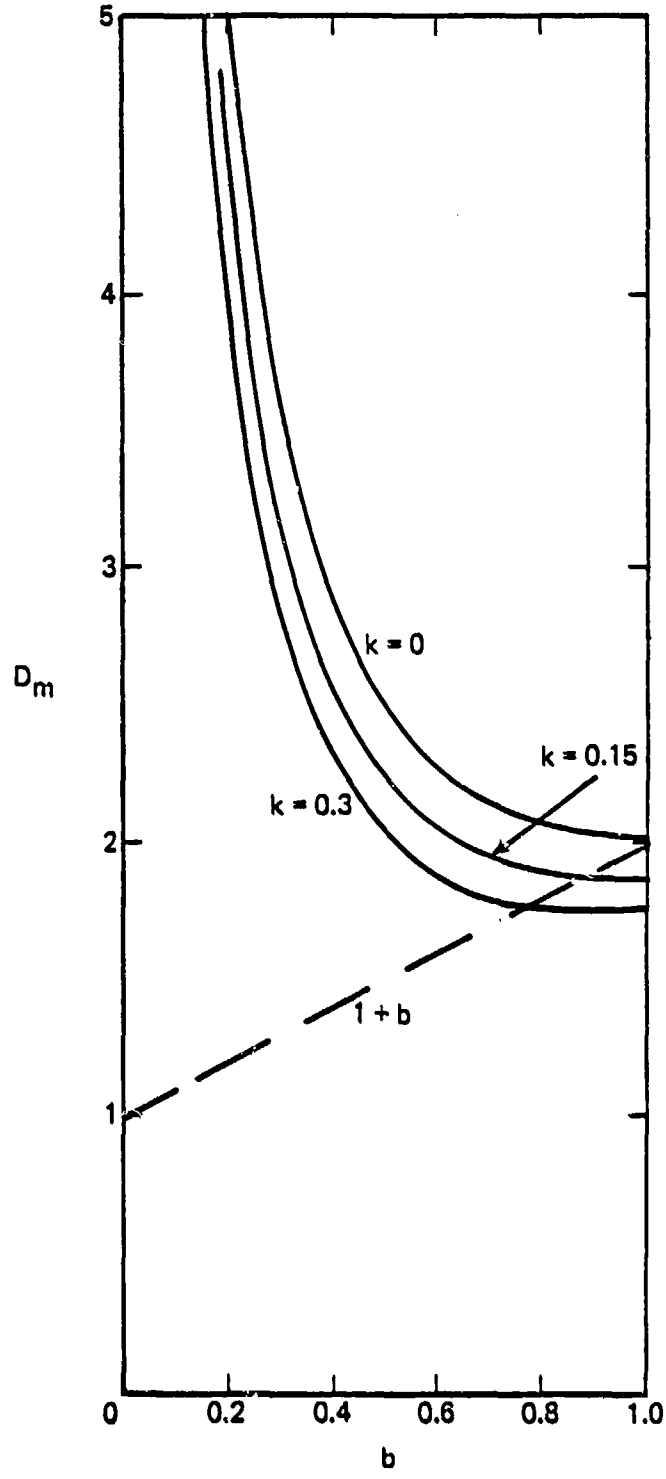

Note: The parameter K is ratio of incoming velocity a fire can overcome over inflow velocity at fire perimeter. Straight line indicates distance D_m for initially touching fires.

Figure 5. Changes in maximum nondimensional distance between fire centers as function of fire radii ratio.

of burn area. The larger fire, assumed fixed in size*, will have an approximate lifetime of

$$\tau_1 = \frac{mC}{JH_f} \quad , \tag{18}$$

which is the time required to burn all the combustible material in the fire area.

The spread rate of the fire at any location is at most approximately equal to the airspeed at that location. On the line connecting the fire centers, which is the line of fastest spread, the speed is, from Eq. (5)

$$u = \frac{B_1}{2\pi r} - \frac{B_2}{2\pi(D - r)} \quad . \tag{19}$$

For a rough estimate of the time required for the fires to merge, one integrates Eq. (19) as

$$\ell = \int_0^{\tau} \frac{B_1}{2\pi} \left[\frac{D - r\left(1 + \frac{B_2}{B_1}\right)}{r(D - r)} \right] dt \quad , \tag{20}$$

where $r = r(t)$ such that $r(0) = D - b$. The result is only approximate since the shape of the merging fires--especially that of the smaller fire--is no longer circular. The induced velocities can no longer be modeled by simple sinks. A numerical marching procedure that adjusts the sink distribution to account for changing (e.g., elliptical) fire areas can be used. When $\ell \geq D - b - 1$, where the large fire initial

*Actually, once the initially smaller fire has grown, and if the initial ratio b was close to unity, it might become the dominant fire and attract the other. This does not change the results shown in Figs. 4 and 5.

radius is unity, the results illustrated in Figs. 4 and 5 are obtained. Otherwise, only partial covering of the areas shown in Fig. 3 is achieved. As the initial areas burn out, the intermediate area continues to spread.

In the case of more than two fires burning simultaneously, the point or points at which the velocity on the perimeter changes direction is not known a priori, as it depends on the two-dimensional positions of the flames, as well as their strength. The velocity at any point can be estimated by considering the following superposition of singularities

$$u = \frac{B_1}{2\pi r_1} + \frac{B_2}{2\pi(r - S_2)} + \frac{B_3}{2\pi(r - S_3)} + \cdots + \frac{B_n}{2\pi(r - S_n)}$$

$$= \sum_{i=1}^{n} \frac{B_n}{2\pi(r - S_i)} , \qquad (21)$$

where r is the distance from the point in question to the center of the fire designated as the "first" fire. The choice is arbitrary and can be made by size or geographical location.

SECTION 4
RESULTS

In this section, we apply the singularity theory to several combinations of area fires and calculate the interactions. A 10-km radius fire serves as a basis for obtaining parameters for a single area fire first, and then for determining multiple area fire interactions (see Sec. 2).

We first consider whether the flow field defined by the calculations can be assumed quasi-steady. Computed ground level flows are 10 m/s at the fire perimeter (Fig. 2) and decay roughly as r^{-1} with distance from the fire center. Thus, far-field inflow speeds of O(1 m/s) are expected, and for distances of $O(10^4$ m), time scales of 10^4 s are obtained.

The fire [calculated by Small, Remetch, and Brode (1984)] is assumed to burn in an area with fuel loading between that of the average urban-suburban combustible load of 40 kg/m^2 [National Academy of Sciences, 1985] and a city such as Hamburg for which the load was estimated at 157 kg/m^2 [Carrier, Fendell, and Feldman, 1985]. The caloric equivalent of those combustibles is $1.86 \cdot 10^7$ J/kg so that the total heat released from the fire per square meter is between $7.44 \cdot 10^8$ and $29.2 \cdot 10^8$ J/m^2. The averaged heat addition rate was 1 kW/m^3 over a height of 100 m so that each square meter of surface area accounts for 100 kW/m^2. Thus, the fire duration is at most from 0.744 to $2.92 \cdot 10^4$ s, i.e., between 2.07 and 8.1 h, depending on the type of area burned. The fire duration is of the same order of magnitude as the characteristic times so that a steady flow is not fully established. Nevertheless, "persistent" (i.e., quasi-steady, slowly changing) patterns appear after ~ 3000 s. Also, the large size of the aggregate fire, which is actually composed of a multitude of smaller fires is assumed to cause averaging of locally periodic buoyant effects [Turner, 1983]. As a result, the velocity field exterior to the fire behaves approximately like a steady flow.

Figure 2 shows the radial inflow calculated at 60 and 90 min after fire initiation. To determine the basic sink distribution strength, we use Eqs. (1) through (3), to calculate the mass and thus the sink strength. For $R = 10^4$ m, $H_f = 10^2$ m, $J = 1$ kW/m^3, and $C = 1.86 \cdot 10^7$ J/kg, $Q = 3.14 \cdot 10^{13}$ J/s and $A = 2.53 \cdot 10^7$ kg/s. Taking the values of the radial inflow at 3600 and 4800 s after the fire start, and an incoming air density of $\rho = 1.2$ kg/m^3, the equivalent sink height is $h = 30$ m. That value describes the region where u is proportional to r^{-1}, and separates the effects of the basic sink distribution from those of the secondary vortices (which appear as a "hump" in the velocity distribution shown in Fig. 2). This hump is the footprint of a concentrated vortex ring that is moving radially outward as time progresses. The biggest increment is observed directly below the vortex ring "core," falling off as $r^{-1} \cos \theta$, where θ is the angle between the vertical and the line connecting each point and the vortex core. In keeping with our model of superposed singularities, the vortex strength is calculated separately below.

The sink height ($h = 30$ m) necessary to provide the air required for the fire is three times less than the 100 m burning zone height, and within the zone over which the inflow velocity does not change with height. The result is consistent with the assumption of a uniform basic sink strength. The sink strength B per unit height, is $B = 8.43 \cdot 10^5$ m^2/s. Thus, the fire has more than 300 percent excess air, so that burning can be unhampered and complete at a height of 100 m.

An alternate estimate of the sink strength can be obtained by kinematic means [Eq. (3)], directly from the velocity curves (outside the fire) of Fig. 2. For an elapsed time of 3600 s, $B = 6.94 \cdot 10^5$ m^2/s (i.e., within 18 percent), and at $t = 4500$ s, $B = 5.26 \cdot 10^5$ m^2/s. Some of the discrepancy might result from our neglect of unsteady effects such as growth and movements of annular vortices. For times shorter than 1 h, however, the starting transient dominates. External speeds of < 15 m/s were calculated so that at 1 h the effect of the fire has only reached $< 5 \cdot 10^4$ m. This can be

clearly seen in the plot of U_i versus r for t = 2700 where the effects of the fire have only reached $\approx 4 \cdot 10^4$ m (see Fig. 6). In any case, agreement between the two independent estimates is encouraging.

The flow around the basic sink is now separated into induced sinks and a vortex. The sink distribution above the fire is again obtained by plotting the horizontal inflow, this time at various heights. For the range 0 to 3000 m, the horizontal velocity exhibits an r^{-1} dependence on $r > 10^4$ m. The results are given in Fig. 7.

The vortex models the turning of lower-level inflow into upper-layer spreading. It is essentially a vortex ring of radius ≈ 18 km at 60 min and ≈ 36 km at 90 min, at a height of ≈ 3 km. The vortex height is approximately halfway between the ground and the major outflow layer, with additional less well-defined vortex-like structures above it. Thus, the vortex ring can be modeled as being constrained between two horizontal planes. This, in turn, is mathematically equivalent to having an infinite row of image vortex rings of alternating direction of rotation with a common axis, equally spaced vertically at about 6 km. The vortices included in the infinite row are essentially reflections of the original ring in the two constraining plumes. The velocity induced by the vortex on the ground is used to establish the vortex strength (see Appendix A).

The vortex strength at 3600 s is $\Gamma = 1600$ m^2/s and its contribution to the velocity field is, at most about 12 percent of the ground velocity. Figure 8 illustrates the ground-level inflow velocity variations from the sink-flow pattern, clearly pinpointing both the vortex (the peak) and the fire edge effect. The outer flow is incompressible, so that the increment in ground-level velocity results from mass coming from above while moving in and moving back upwards at radial distances less than the instantaneous vortex position. The difference between the calculated ground flow and sink flow at 4800 s is that the vortex has moved out to ~ 36 km and another vortex is forming at 15 to 16 km from the fire center (still relatively weak). The strength of the original vortex is unchanged (its height is constant and the maximal induced velocity has changed by less than

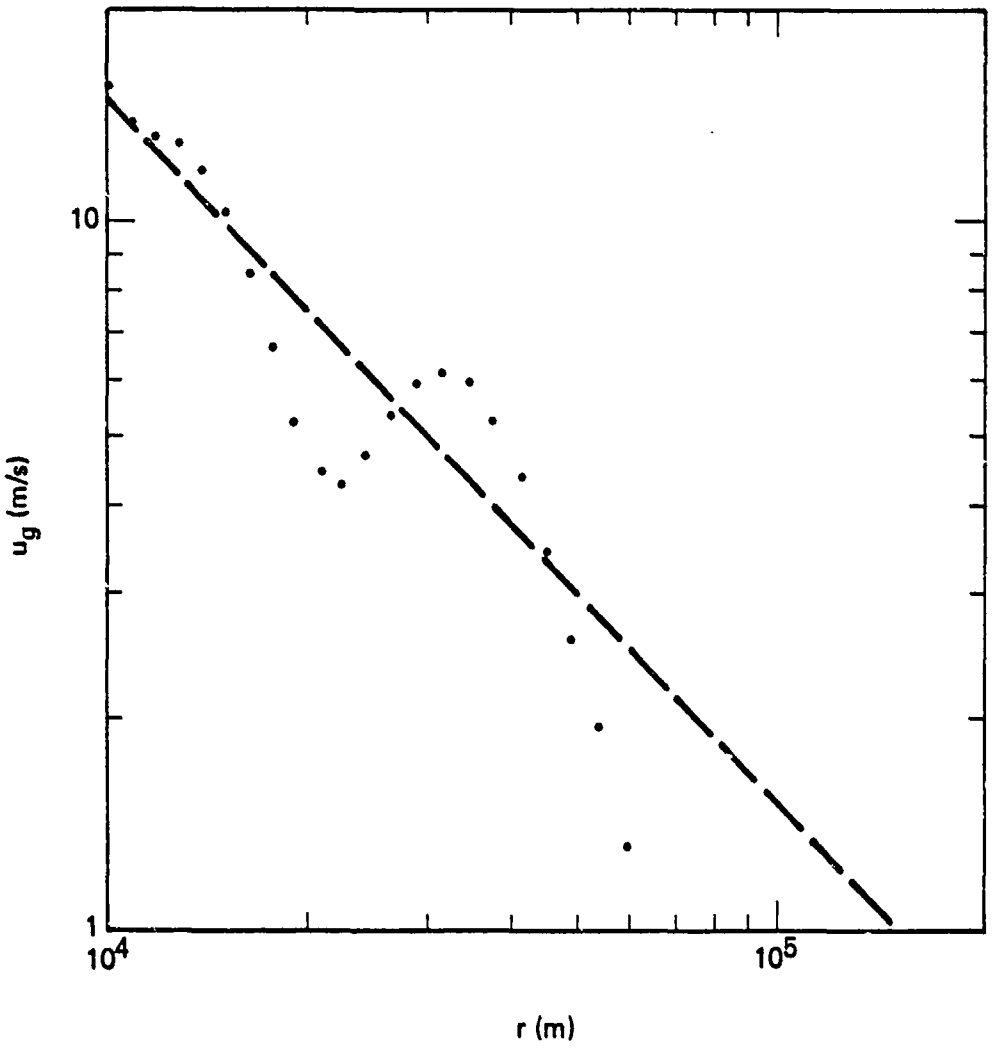

Figure 6. Radial velocity of ground level at t = 2700 s.

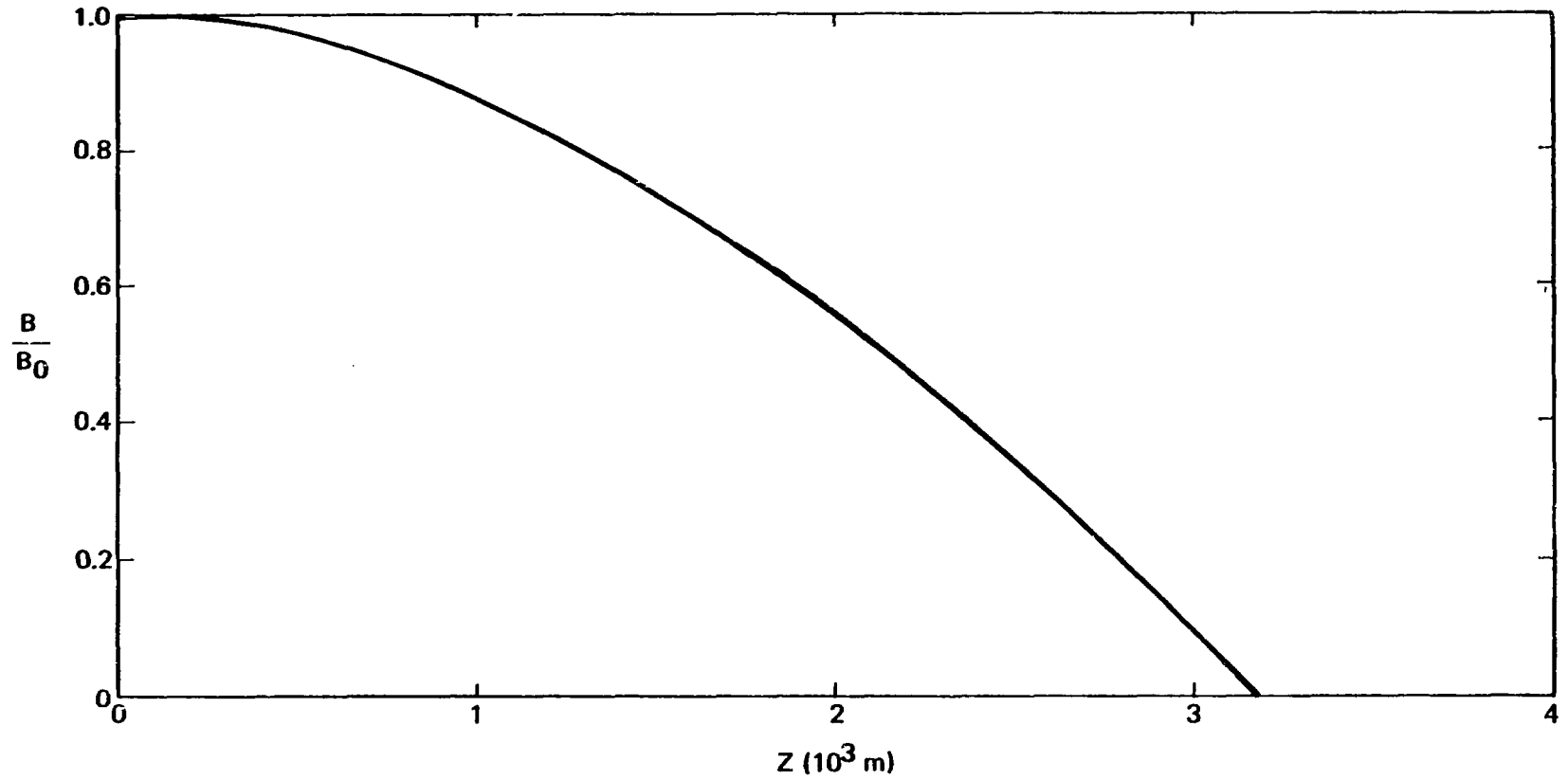

Note: The sink strength per unit height is normalized by the "basic" sink strength for a 10-km fire (see Fig. 2).

Figure 7. Distributed induced sink strength versus height at t = 3600 s.

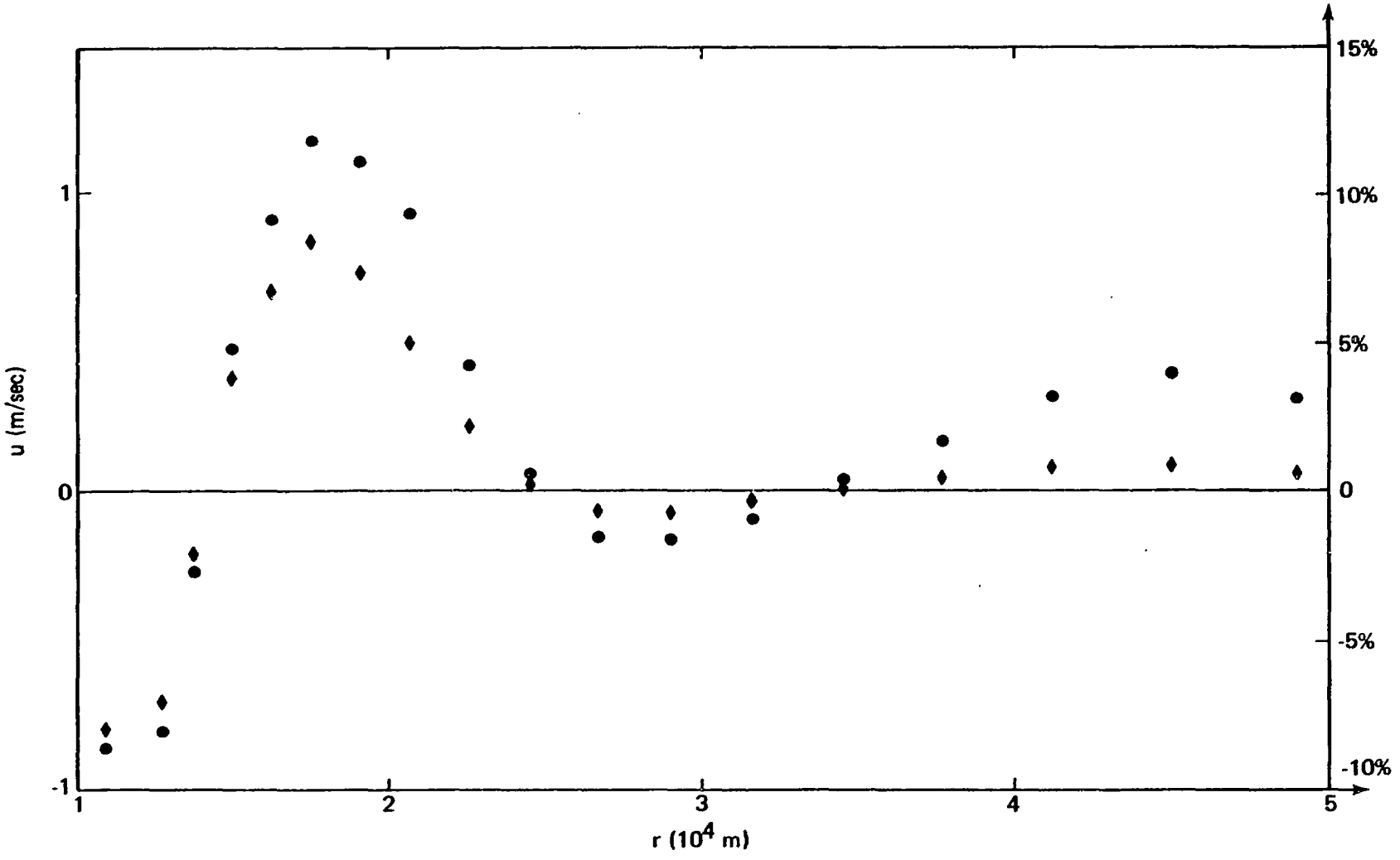

Note: Diamonds indicate absolute values and circles indicate percent of total velocity.

Figure 8. Radial velocity at ground level for fire at 3600 s from inception with basic sink flow subtracted.

5 percent to slightly above 0.8 m/s). The center of vorticity is moving radially outward at an average speed of 10 m/s during the period 3600 to 4800 s after inception (an indication of the growth of the cloud of combustion products near the tropopause).

Figure 9a illustrates the ground-level flow field generated by a configuration of three fires all burning an area of uniform combustible density. The strength (mass burned per unit time) of the two smaller fires (Nos. 2 and 3) is 36 percent of the larger fire (proportional to the radii ratio squared). The streamlines between fires 1 and 2, and 1 and 3, respectively, are similar, and suggest a burn pattern such as sketched in Fig. 3. In contrast, Fig. 9b illustrates a case in which fire 2 is attracted to fire 1, but fire 3 is not attracted to fire 1. Thus a burning corridor is established only between fires 1 and 2. That illustrates the effect of intensity on merging of area fires.

Figures 9c-d show a different placement of the three bursts (and fires) described in Figs. 9a-b. In Fig. 9d, fire 3 burns a similar size area but with twice the combustible loading. Fire 2 is attracted to fire 3 and not to the larger fire 1. Those results illustrate the influence of parameters such as fire areas, relative positions, and fire strengths on the stability of an area fire or system of area fires. The configuration shown in Fig. 9a leads to a superfire encompassing all the initial fires. Alternatively, three fires (Fig. 9c) similar in size to those in Fig. 9a, remain separate. In those cases, the relative positions determine whether the fires merge. The comparisons of both Figs. 9a-b and Figs. 9c-d illustrate the influence of area fire intensity or strength. A heavier fuel loading in one district may cause merging. Similarly, different burst times may lead to merging due to unequal (at least initially) burn rates. Those results suggest that multiburst optimization procedures can be applied to maximize or minimize the burned area.

It should be mentioned that the calculations shown in Figs. 9a-d are instantaneous pictures of each fire flow field. After two or more fires have produced burning corridors or merged, the total sink

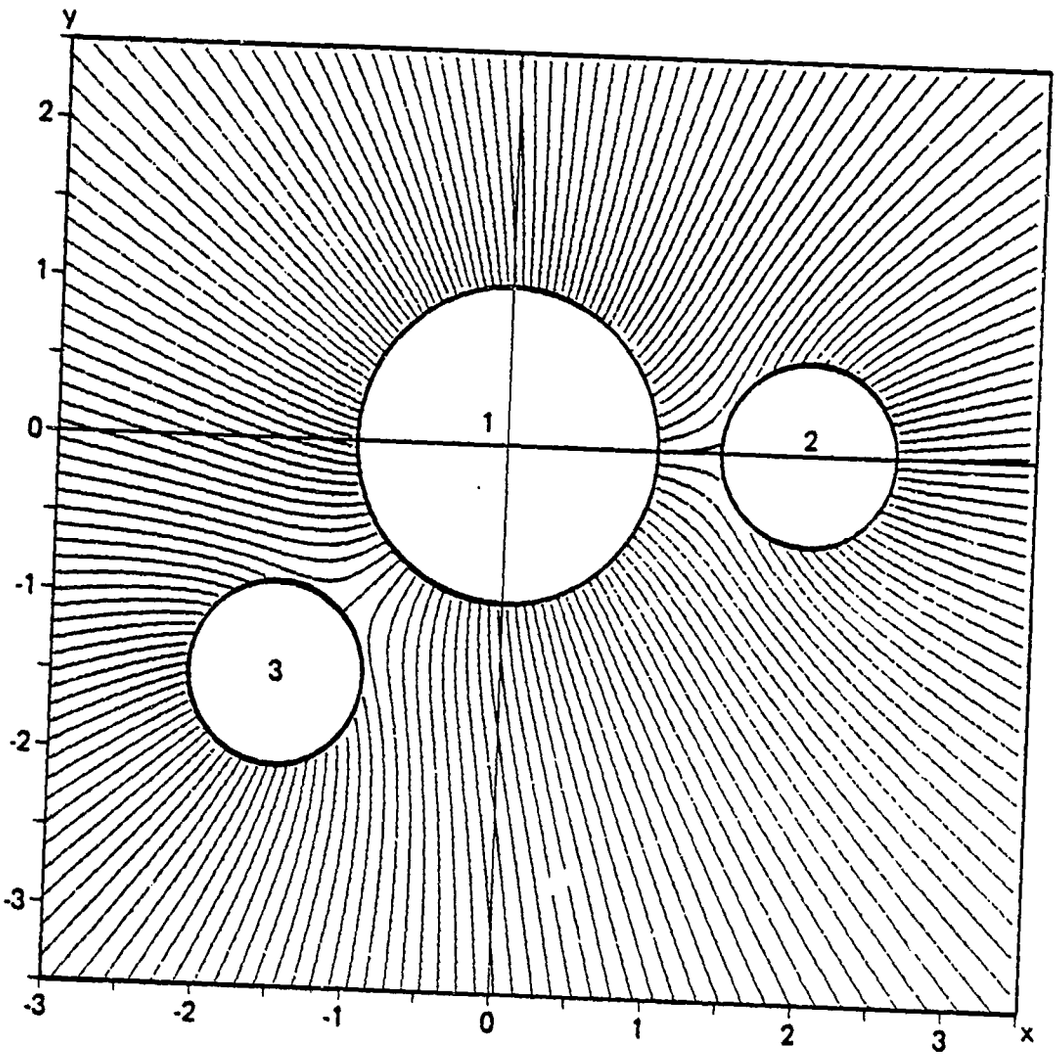

Burst	X-center	Y-center	Radius	Strength
1	0.00	0.00	1.00	1.00
2	2.00	0.00	0.58	0.33
3	-1.50	-1.50	0.58	0.33

a. All area fires merge.

Note: Fires 2 and 3 have radii 60 percent that of fire 1, and all burn in a uniform area (equal combustible quantity per unit area).

Figure 9. Ground level flow-field streamlines for three fires in proximity.

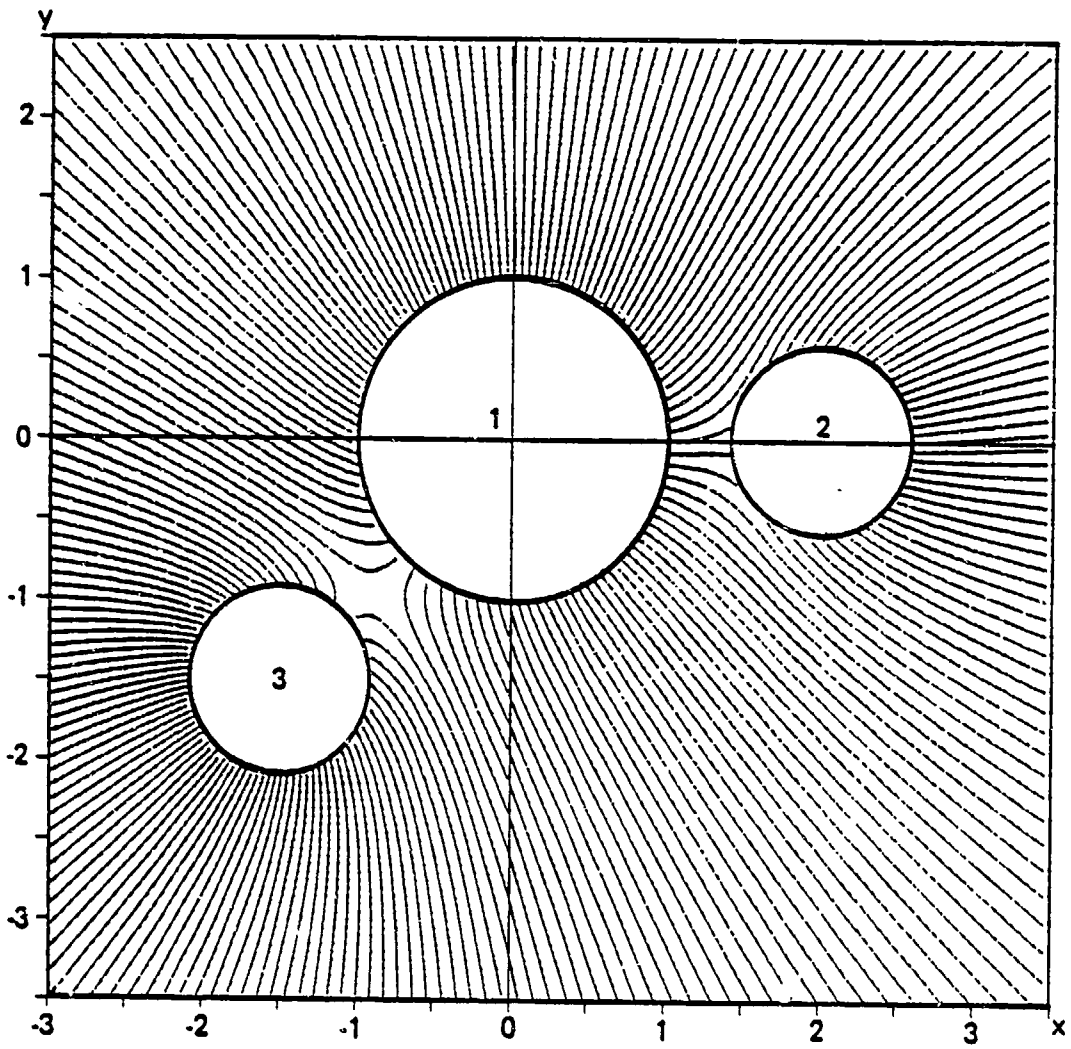

Burst	X-center	Y-center	Radius	Strength
1	0.00	0.00	1.00	1.00
2	2.00	0.00	0.58	0.33
3	-1.50	-1.50	0.58	0.67

b. Fires 1 and 2 merge; fire 3 remains separate.

Note: Fire 3 burns twice the combustible per unit area and time as the other fires.

Figure 9. Ground level flow-field streamlines for three fires in proximity (Continued).

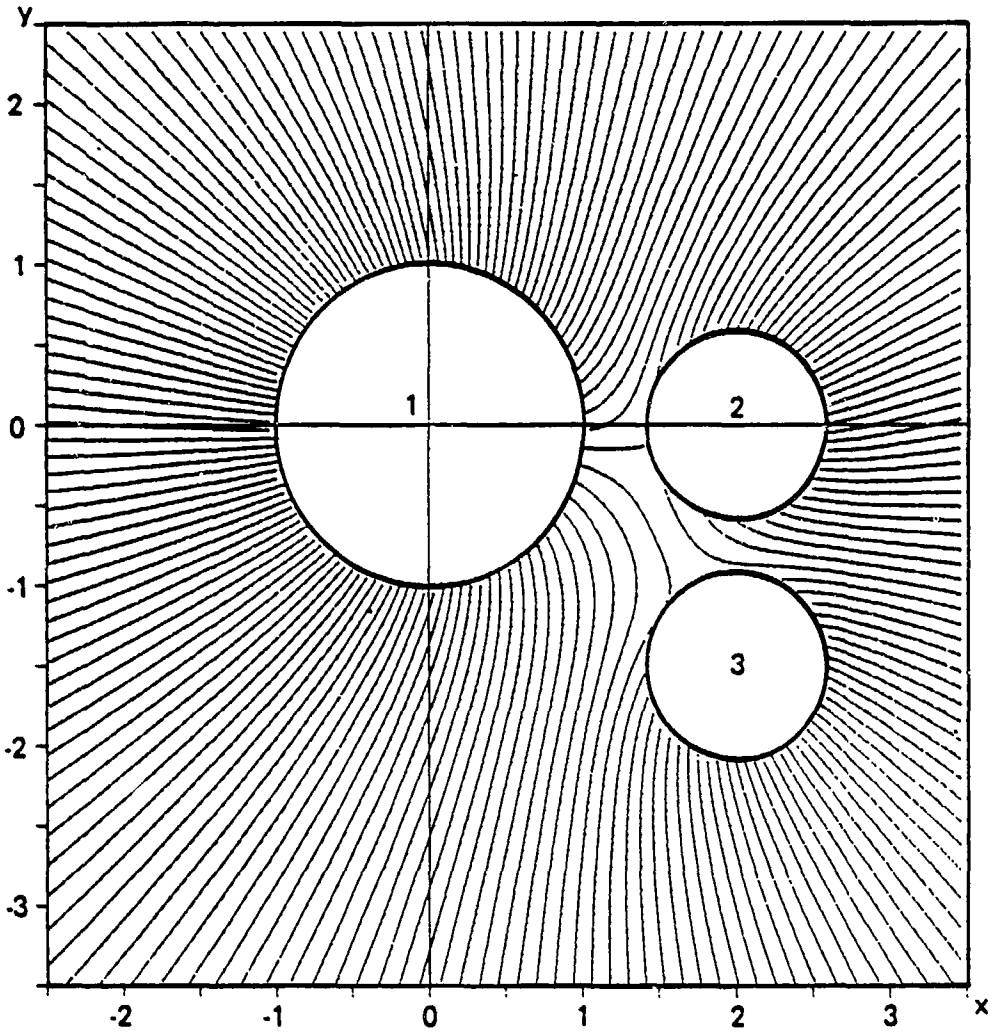

Burst	X-center	Y-center	Radius	Strength
1	0.00	0.00	1.00	1.00
2	2.00	0.00	0.58	0.33
3	2.00	-1.50	0.58	0.33

c. All area fires remain separate.

Note: Fires 2 and 3 have radii 60 percent that of fire 1, and all burn in a uniform area (equal combustible quantity per unit area).

Figure 9. Ground level flow-field streamlines for three fires in proximity (Continued).

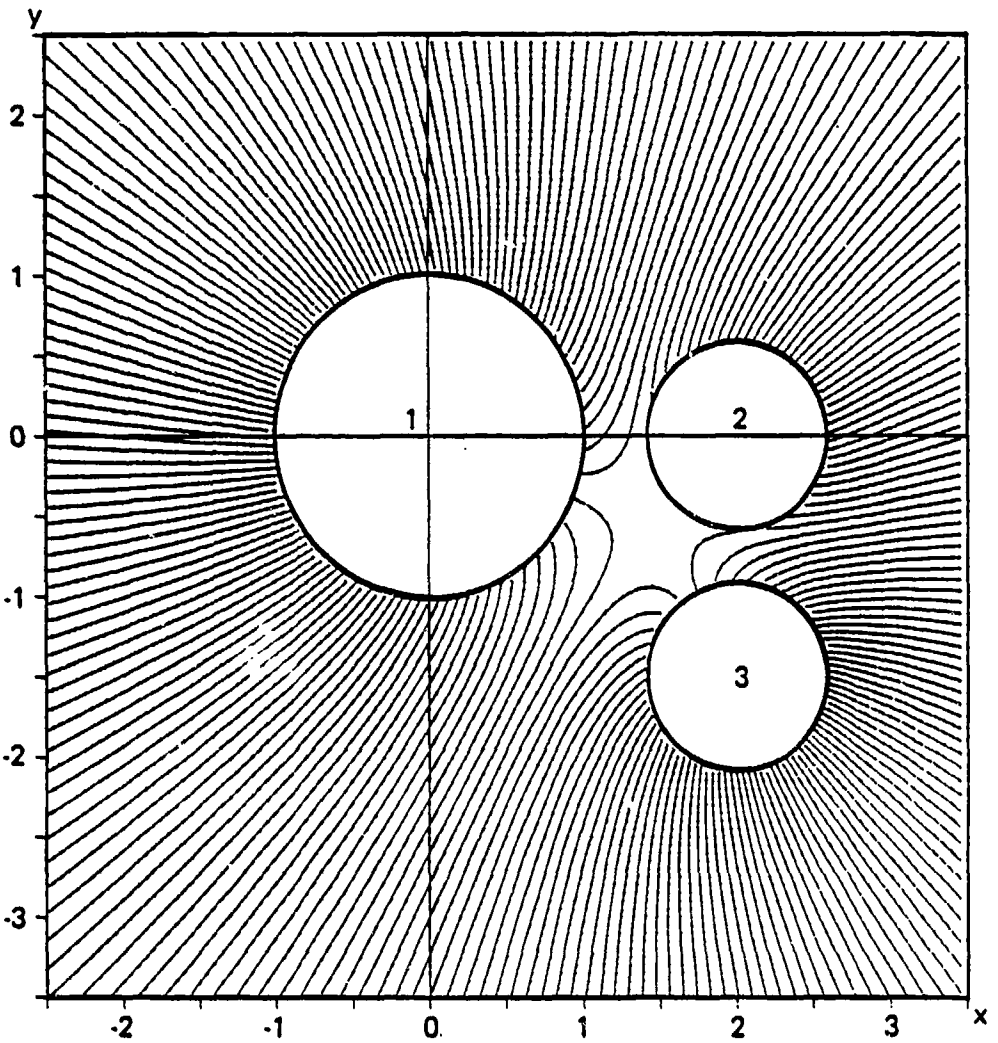

Burst	X-center	Y-center	Radius	Strength
1	0.00	0.00	1.00	1.00
2	2.00	0.00	0.58	0.33
3	2.00	-1.50	0.58	0.67

d. Fires 2 and 3 merge; fire 1 remains separate.

Note: Fire 3 now burns twice the combustible per unit area and time as the other fires.

Figure 9. Ground level flow-field streamlines for three fires in proximity (Concluded).

strength changes, which can result in a change in the flow (streamline) pattern and thus the burning pattern. An integration procedure can be devised to account for the quasi-steady changes in the fire sizes and shapes.

All the above calculations assume $V_o = 0$. A rough estimate of the maximum inflow velocity V_o which a fire can overcome and spread upwind, can be drawn by using the criteria suggested in Glasstone and Dolan [1977]. The best current estimate requires a wind of less than 8 mph. That translates to less than 3.6 m/s or $K < 0.28$, i.e., within the parameter range given in Fig. 5.

SECTION 5
CONCLUSIONS

Hydrodynamic considerations show that large area fires can interact when in proximity. Single large area fires are usually characterized by a fixed position and a quasi-steady radial inflow of ground-level air. The flow field inhibits spreading in a solitary fire, but when two or more unequal fires are within a few radii of each other, the larger or more intense fire can "attract" smaller or weaker fires, causing (for two fires) an increase of up to 50 percent in total burned area. That effect is greatest when the ratio of fire sizes is about 3, or when they are ~ 3 large fire radii apart. That interaction can be multiplied if more than one small fire is near a large fire. Similar interactions occur for fires of equal size, but with different burning ratios (combustible loads).

Our conclusions hold for simultaneously burning fires. Different merge criteria apply for fires starting to burn in the vicinity of an established large area fire. Preliminary considerations suggest that the configurations similar to those illustrated in Fig. 3b will be obtained, with much larger separations still leading to fire coalescence. Such time-dependent effects, as well as area fire configurations representative of lay downs in actual urban areas will be considered in a future PSR study.

SECTION 6

LIST OF REFERENCES

Bond, H., ed., Fire and the Air War, National Fire Protection Association, Boston, Massachusetts, 1951.

Carrier, G. F., F. E. Fendell, and P. S. Feldman, "Firestorms," J. Heat Trans., Vol. 107, 1985, pp. 19-27.

Cox, G., and R. Chitty, "A Study of the Deterministic Properties of Unbounded Fire Plumes," Combustion and Flame, Vol. 39, 1980, pp. 191-209.

Emmons, H. W., "Fundamental Problems of the Free Burning Fire," Tenth International Symposium on Combustion, Combustion Institute, Pittsburgh, Pennsylvania, 1965, pp. 951-964.

Glasstone, S., and P. J. Dolan (eds.), The Effects of Nuclear Weapons, U.S. Department of Defense, Washington, DC, 1977.

Irving, D., Destruction of Dresden, William Kimber and Co., Ltd., London, England, 1963.

Lamb, Sir Horace, Hydrodynamics, 6th ed., Dover Publications, Inc., New York City, 1945.

Miller, C. F., Summary of Damage Inflicted by Air Raids on the City of Hamburg in the Period July 25 to August 3, 1943, NRDL-TRC-68-30, July 1968.

Nielsen, H. J., Mass Fire Analysis, IIT Research Institute, Chicago, Illinois, Report 2018, 1970.

National Academy of Sciences, National Research Council, The Effects on the Atmosphere of a Major Nuclear Exchange, National Academy Press, Washington, DC, 1985.

Small, R. D., and D. A. Larson, "Velocity Fields Generated by Large Fires," Israel J. Technol., 1986 (subsequently published in Proceedings 26th Israel Annual Conference, February 8-9, 1984).

Small, R. D., D. Remetch, and H. L. Brode, "The Physics of Large Fires," Proceedings: Conference on Large Scale Fire Phenomenology, Gaithersburg, Maryland, September 1984.

Small, R. D., Observations of the Chapleau-Canada Test Fire, Pacific-Sierra Research Corporation, Memo, August 1985.

Smith, R. H., B. R. Morton, and L. M. Leslie, "The Role of Dynamic Pressure on Generating Firewinds," J. Fluid Mech., Vol. 68, 1975, pp. 1-19.

Turner, J. S., Buoyancy Effects in Fluids, Cambridge University Press, New York City, 1973.

Nielsen, H. J., and L. N. Tao, "The Fire Plume Above a Large Free-Burning Fire," Tenth International Symposium on Combustion, The Combustion Institute, 1965, pp. 965-972.

Weihs, D., and R. D. Small, Swirl Induced by Large Area Fires, Pacific-Sierra Research Corporation, Note 676, 1 October 1985.

APPENDIX A

CALCULATION OF VORTEX STRENGTH

The strength of the vortex used to model the flow outside of the fire plume is obtained by an inverse technique using the velocity induced at the ground. The stream function describing flow outside of an isolated vortex ring is [Lamb, 1932]

$$\psi = \frac{\Gamma}{2\pi}(r_1 + r_2)[F_1(\lambda) - E_1(\lambda)] \quad , \tag{22}$$

where r_1 and r_2 are the least and greatest distances from the point in question to elements of the ring, $\lambda = r_2 - r_1(r_2 + r_1)$, and F_1 and E_1 are the complete elliptic integrals of the first and second kind, respectively. Equation (22) may now be used as a basis for generating the velocity due to the infinite column of image vortices by summation. The radial velocity at the ground is obtained as the derivative

$$u = \frac{1}{r}\frac{\partial \psi}{\partial z} \quad . \tag{23}$$

A great simplification in the calculation is made by assuming that the flow field directly beneath the ring vortex is a rectilinear vortex. That assumption introduces only small inaccuracies, as the radius of the ring vortex (~ 15 to 30 km) is much greater than the vertical distance of the point in question - 3 km (directly beneath one element) and the error is proportional to the inverse of the ratio. The simplified calculation is presented here to describe the process used for the ring vortices.

The complex potential of a single line vortex at point (0, ia) is $-i\Gamma \ell n(z - ia)$ where z is the complex variable $z = x + iy$. The images appear as vortices of opposite sign at (0, - ia + 4 na) and of the same sign at (0, ia + 4 na) where n goes from $-\infty$ to $+\infty$ so that the complex potential is

$$W = -\sum_{n=-\infty}^{\infty} [i\Gamma \ell n(z - ia - 4na) - i\Gamma \ell n(z + ia - 4na)] ,$$

$$= -i\Gamma \ell n \sin h \frac{\pi z}{4a} - \ell n \sin h \frac{\pi(z - 2ia)}{4a} ,$$

$$= -i\Gamma \left(\ell n \frac{\sin h \frac{\pi z}{4a}}{\sin h \frac{\pi(z - 2ia)}{4a}} \right) . \qquad (24)$$

The velocity induced directly beneath the vortex center is

$$u = 2 \sum_{n=0}^{\infty} \left(\frac{\Gamma}{a + 4na} - \frac{\Gamma}{3a + 4na} \right) ,$$

$$= \frac{2\Gamma}{a} \sum_{n=0}^{\infty} \frac{(-1)^n}{2n + 1} ,$$

$$= \frac{\Gamma \pi}{2a} . \qquad (25)$$

The induced velocity is 57 percent higher than for a single vortex. That factor can be alternatively understood as resulting from "squeezing" the flow by constraining it to move parallel to the ground. The greatest velocity increment is about 0.84 m/s (Fig. 8) so that for the height of a = 3000 m, we obtain $\Gamma = 1600$ m^2/s [Eq. (25)].

APPENDIX B
LIST OF SYMBOLS

$\dot{A}$ = air mass inflow rate [MT^{-2}]

B = sink strength per unit length [M/LT]

b = ratio of radii of small fire to large fire

C = average caloric value of combustibles [L^2T^{-2}]

D = maximum distance for definite spreading [L]

D_m = maximum distance for definite spreading [L]

F = defined in Eq. (13)

h = height of basic sink distribution, simulating air inflow [L]

H = plume final height [L]

H_f = flame zone height [L]

J = heat addition ratio per unit time and volume [$ML^{-1}T^{-3}$]

K = defined by Eq. (15)

m = combustible mass per unit area burned [ML^{-2}]

Q_f = total energy converted per unit time, by fire. [ML^2T^{-3}]

r = radial coordinate [L]

R = flame zone radius [L]

S = air/fuel ratio of fire [0]

t = time

u = radial speed

u_g = radial speed at ground level [L/T]

u_p = velocity at point p [see Eq. (6)] [L/T]

V_f = flame zone volume [L^3]

z = vertical coordinate [L]

θ = angular coordinate

τ = fire lifetime

DISTRIBUTION LIST

DEPARTMENT OF DEFENSE

DEFENSE INTELLIGENCE AGENCY
ATTN: DB-6E2 C WIEHLE
ATTN: RTS-2B
ATTN: WDB-4CR

DEFENSE NUCLEAR AGENCY
ATTN: RAAE
2 CYS ATTN: SPTD
ATTN: STSP
4 CYS ATTN: STTI-CA

DEFENSE TECHNICAL INFORMATION CENTER
12 CYS ATTN: DD

FIELD COMMAND DEFENSE NUCLEAR AGENCY
ATTN: FCTT W SUMMA
ATTN: FCTXE

JOINT STRAT TGT PLANNING STAFF
ATTN: JLKS

DEPARTMENT OF ENERGY

UNIVERSITY OF CALIFORNIA
LAWRENCE LIVERMORE NATIONAL LAB
ATTN: J BACHOVSKY
ATTN: N ALVAREZ
ATTN: R PERRETT

LOS ALAMOS NATIONAL LABORATORY
ATTN: DR. D CAGLIOSTRO

OTHER GOVERNMENT

DEPARTMENT OF COMMERCE
ATTN: H BAUM
ATTN: R LEVINE

DIRECTOR, FFASR
ATTN: C CHANDLER

FEDERAL EMERGENCY MANAGEMENT AGENCY
ATTN: H TOVEY
ATTN: OFC OF RSCH/NP H TOVEY

OFFICE OF EMERGENCY SERVICES
ATTN: W TONGUET

DEPARTMENT OF DEFENSE CONTRACTORS

CALIFORNIA RESEARCH & TECHNOLOGY, INC
ATTN: M ROSENBLATT

CARPENTER RESEARCH CORP
ATTN: H J CARPENTER

CHARLES SCAWTHORN
ATTN: C SCAWTHORN

FACTORY MUTUAL RESEARCH CORP
ATTN: R FRIEDMAN

IIT RESEARCH INSTITUTE
ATTN: H NAPADENSKY

INSTITUTE FOR DEFENSE ANALYSES
ATTN: L SCHMIDT

KAMAN SCIENCES CORP
ATTN: E CONRAD

KAMAN TEMPO
ATTN: DASIAC

KAMAN TEMPO
ATTN: DASIAC

MISSION RESEARCH CORP
ATTN: J BALL

MODELING SYSTEM, INC
ATTN: G BERLIN

NOTRE DAME DU LAC, UNIV OF
ATTN: T J MASON

PACIFIC-SIERRA RESEARCH CORP
2 CYS ATTN: D WEIHS
ATTN: H BRODE, CHAIRMAN SAGE
2 CYS ATTN: R SMALL

R & D ASSOCIATES
ATTN: D HOLLIDAY
ATTN: F GILMORE
ATTN: R TURCO

RAND CORP
ATTN: P DAVIS

RAND CORP
ATTN: B BENNETT

SCIENCE APPLICATIONS INTL CORP
ATTN: M DRAKE
ATTN: M MCKAY

SCIENCE APPLICATIONS INTL CORP
ATTN: J COCKAYNE

SCIENTIFIC SERVICES, INC
ATTN: C WILTON

SRI INTERNATIONAL
ATTN: G ABRAHAMSON

STAN MARTIN ASSOCIATES
ATTN: S MARTIN

SWETL, INC
ATTN: T PALMER

TRW ELECTRONICS & DEFENSE SECTOR
ATTN: F FENDELL